Kohnert, K., Juhls, B., Muster, S., Antonova, S., Serafimovich, A., Metzger, S., Hartmann, J., Sachs, T. (2018): Toward understanding the contribution of waterbodies to the methane emissions of a permafrost landscape on a regional scale-A case study from the Mackenzie Delta, Canada. - Global Change Biology, 24, 9, 3976-3989.

https://doi.org/10.1111/gcb.14289

Towards Understanding the Contribution of Waterbodies to the Methane Emissions of a Permafrost Landscape on a Regional Scale – A Case Study from the Mackenzie Delta, Canada

Running head: **Regional CH_4 flux from arctic waterbodies**

Katrin Kohnert[1], Bennet Juhls[1,2], Sina Muster[3], Sofia Antonova[3,4], Andrei Serafimovich[1], Stefan Metzger[5,6], Jörg Hartmann[7], Torsten Sachs[1,8]

1. GFZ German Research Centre for Geosciences, Telegrafenberg, 14473 Potsdam, Germany
2. Now at: Institute for Space Sciences, Department of Earth Sciences, Freie Universität Berlin, Carl-Heinrich-Becker-Weg 6–10, 12165 Berlin, Germany
3. Alfred Wegener Institute, Helmholtz Centre for Polar and Marine Research, 14473 Potsdam, Germany
4. GIScience, Department of Geography, Heidelberg University, Heidelberg, 69120, Germany
5. National Ecological Observatory Network, Battelle, 1685 38th Street, Boulder, CO 80301, USA
6. University of Wisconsin-Madison, Dept. of Atmospheric and Oceanic Sciences, 1225 West Dayton Street, Madison, WI 53706, USA
7. Alfred Wegener Institute Helmholtz Centre for Polar and Marine Research, Am Handelshafen 12, 27570 Bremerhaven, Germany
8. Institute of Flight Guidance, TU Braunschweig, Hermann-Blenk-Str. 27, 38108 Braunschweig, Germany

Correspondence: K. Kohnert, tel. +49 331 288 28847, e-mail: katrin.kohnert@gfz-potsdam.de and T. Sachs, tel. +49 331 288 1423, e-mail: torsten.sachs@gfz-potsdam.de

Keywords: airborne eddy-covariance, CH_4, Arctic, TerraSAR-X, Sentinel-1, remote sensing, lakes, ponds

Type of paper: primary research article

Abstract

Waterbodies in the arctic permafrost zone are considered a major source of the greenhouse gas methane (CH_4) in addition to CH_4 emissions from arctic wetlands. However, the spatio-temporal variability of CH_4 fluxes from waterbodies complicates spatial extrapolation of CH_4 measurements from single waterbodies. Therefore, their contribution to the CH_4 budget of the arctic permafrost zone is not yet well understood. Using the example of two study areas of 1,000 km^2 each in the Mackenzie Delta, Canada, we approach this issue i) by analyzing correlations on the landscape scale between numerous waterbodies and CH_4 fluxes and ii) by analyzing the influence of the spatial resolution of CH_4 flux data on the detected relationships. A CH_4 flux map with a resolution of 100 m was derived from two aircraft eddy-covariance campaigns in the summers of 2012 and 2013. We combined the CH_4 flux map with high spatial resolution (2.5 m) waterbody maps from the Permafrost Region Pond and Lake Database and classified the waterbody depth based on Sentinel-1 SAR backscatter data. Subsequently, we reduced the resolution of the CH_4 flux map to analyze if different spatial resolutions of CH_4 flux data affected the detectability of relationships between waterbody coverage, number, depth, or size and the CH_4 flux. We did not find consistent correlations between waterbody characteristics and the CH_4 flux in the two study areas across the different resolutions. Our results indicate that waterbodies in permafrost landscapes, even if they seem to be emission hotspots on an individual basis or contain zones of above average emissions, do currently not necessarily translate into significant CH_4 emission hotspots on a regional scale, but their role might change in a warmer climate.

Introduction

Arctic permafrost landscapes with extensive wetlands and numerous waterbodies are considered an important source of the greenhouse gas methane (CH_4) (e.g. Schuur *et al.*, 2015; Walter *et al*., 2006; Wik *et al.*, 2016b). Annual CH_4 emissions from the Arctic are estimated to contribute between 32 Tg and 112 Tg (McGuire et al., 2009) to the 500 Tg to 600 Tg CH_4 emitted globally per year (Dlugokencky *et al.*, 2011). In addition to this large range in CH_4 emissions from the Arctic, further uncertainty of theses regions' CH_4 emissions is introduced by emissions from waterbodies, such as lakes and ponds (Wik *et al*., 2016a; Wik *et al*., 2016b). Globally arctic permafrost lowlands are characterized by the highest number of lakes and the largest fraction of the terrestrial surface covered by waterbodies (Lehner and Döll, 2004; Smith *et al*., 2007; Verpoorter *et al*., 2014). Therefore, we need to understand the regional contribution and relevance of these CH_4 emissions to assess regional CH_4 budgets. Currently, the contribution of waterbodies to the CH_4 budget on a regional or global scale is not yet well determined i) due to the high spatial heterogeneity of CH_4 fluxes (Saunois *et al*., 2016; Wik *et al*., 2016a; Natchimuthu *et al*., 2015) and ii) due to methodological constraints (Thornton *et al*., 2016; Wik *et al*., 2016a; Melton *et al*., 2013).

The high spatial heterogeneity of CH_4 fluxes from waterbodies is conditioned by the heterogeneity of waterbody characteristics, such as size and depth (Wik *et al*., 2016b; Natchimuthu *et al*., 2015, Bastviken *et al*., 2004) or temperature (Yvon-Durocher *et al*., 2014). Studies performed at individual waterbodies have found relations between those waterbody characteristics and the CH_4 flux that are used for pan-Arctic spatial extrapolation. Extrapolation studies assume, for example, a positive correlation between waterbody depth and area (Wik *et al*., 2016b; Natchimuthu *et al*., 2015, Bastviken *et al*., 2004) as described on a waterbody scale (Langer *et al*., 2015). Especially small ponds can be exceptionally strong CH_4 sources per unit area (Wik *et al*., 2016b, Holgerson and Raymond, 2016, Laurion *et al*.,

2010), due to limited opportunity for oxidation in the water column (Bastviken *et al*., 2002), higher water temperatures, more CH_4 production (Yvon-Durocher *et al*., 2014) than in deep waterbodies, and a large margin to area ratio with more decomposable organic material at the waterbody shores (Walter Anthony *et al*., 2016). Additionally, ebullition (bubbling) events especially occur in small waterbodies due to smaller hydrostatic pressure compared to deep waterbodies (Rasilo *et al*., 2015; Bastviken *et al*., 2004). The contribution of small waterbodies to the CH_4 flux is likely to increase in warmer conditions through thermal erosion of the shores leading to an increased availability of organic material (Laurion *et al*., 2010). In contrast, large waterbodies tend to emit less CH_4 than small waterbodies on a unit area, but play a larger role on a regional scale conditioned by their large combined areal extent (Wik *et al*., 2016b). Spatial heterogeneity can be increased further by certain processes occurring in permafrost regions such as thermokarst and the formation of taliks (thaw bulbs) beneath waterbodies that do not freeze to the bottom during the cold season. Thermokarst lakes are especially strong sources of CH_4 (Walter *et al*., 2006, Wik *et al*., 2016b) as their degrading shores provide new organic material for microbial decomposition (Walter Anthony *et al*., 2016). In the unfrozen organic material of taliks, year-round CH_4 production is possible. Moreover, taliks may connect to deeper hydrocarbon reservoirs with old, geologic CH_4, that was created by past microbial decomposition or thermogenic processes (Walter Anthony *et al*., 2012).

In addition to the spatial heterogeneity, Thornton *et al*. (2016) identified several methodological constraints that need to be solved before CH_4 emissions from permafrost waterbodies are sufficiently understood and can be projected into the future. Previously, the spatial resolution of waterbody mapping has been too coarse to include small lakes and ponds. Regional upscaling efforts based on such coarse land cover information therefore exclude a potentially large source of CH_4. Moreover, a coarse resolution of land cover classes together

with the imprecise definition of wetlands can lead to double-counting of emissions from ponds and wetlands. Thornton *et al*. (2016) propose that this double-counting might be a reason why pan-Arctic bottom-up flux estimates are about twice as high as top-down estimates.

Overall, a spatial extrapolation of CH_4 fluxes from waterbodies to the pan-Arctic, a country or even a region containing a variety of waterbodies is still associated with large uncertainties (Saunois *et al*., 2016). For a more reliable regional extrapolation, discrimination of CH_4 fluxes from inland waters is strongly needed, which is possible through more representative CH_4 measurements and improved waterbody mapping databases (Saunois *et al*., 2016). We contribute to this by analyzing connections between highly resolved waterbody types, defined by their depth and area, and CH_4 fluxes that have been measured on regional scale in two 1,000 km^2 large study areas in the waterbody-rich Mackenzie Delta in the Canadian Arctic.

The objectives of this study are to advance our understanding of the contribution of the CH_4 emissions from waterbodies to a region's CH_4 budget and further to understand the role of the spatial resolution of the CH_4 measurements. We address the following questions:

1. Are there relations between waterbody characteristics and CH_4 flux that exist independently from the spatial resolution of the CH_4 measurements?
2. Do CH_4 emissions from waterbodies exceed those form the surrounding land surface?
3. Are CH_4 emissions larger in areas with a large number of shallow or small lakes?
4. How do the Mackenzie Delta CH_4 fluxes compare to fluxes reported from the circum-Arctic?

Methods

Study area

The study areas are located in the Mackenzie Delta in the Canadian Arctic (67°26'N – 69°33'N, 133°22'W – 136°30'W; Fig. 1a), the second largest arctic river delta covering 13,000 km². The permafrost in the delta is classified as discontinuous and is up to 100 m thick (Burn & Kokelj, 2009). A transition from taiga to tundra occurs between 68°30'N and 69°30'N (Burn & Kokelj, 2009). The Mackenzie Delta is located in a zone of medium to high soil organic carbon content (50-70 kg m^{-2}) in the upper 1 m as classified by Hugelius *et al.* (2014). During the Last Glacial Maximum, the study area was at the margin of the Laurentide ice sheet (Jakobsson et al., 2014). The present Mackenzie Delta developed through fluvial processes into a basin covered by seawater that later emerged above sea level during the Holocene (Carson *et al*., 1999; Taylor *et al*., 1996). The Big Lake Delta Plain, east of the northern part of the main delta was not submerged during the Wisconsinan glaciation, but was covered with water during the Holocene due to sea level rise and thermokarst processes, before sedimentation lead to its re-emerging (Taylor *et al*., 1996). Large portions of the surface are covered with lakes, ranging from < 15 % surface coverage in the north, to 15-30 % in the south and 30-50 % in the middle of the delta (Mackay, 1963). In total, the Mackenzie Delta contains more than 49,000 waterbodies (Emmerton *et al*., 2007). Through-taliks are common below waterbodies in the Mackenzie Delta (Ensom *et al*., 2012; Burn, 2002; Burn & Kokelj, 2009). The ice thickness in river channels and waterbodies during winter is less than 2 m (Sanden *et al*., 2009; Marsh, 1991). Emissions of old, geologic CH_4 from subsurface reservoirs located below the northern Mackenzie Delta contribute strongly to the region's annual CH_4 budget (Kohnert *et al.*, 2017).

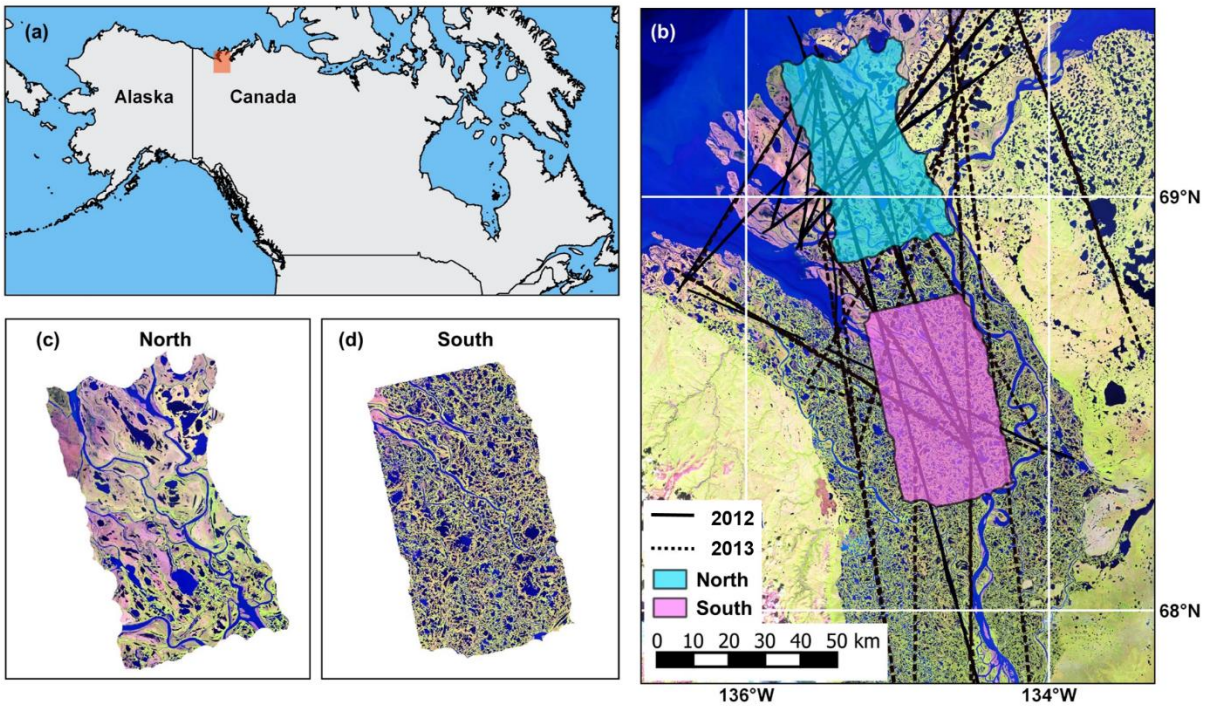

Fig. 1: Location and land cover of the two study areas "North" and "South" in the Mackenzie Delta, Canada. Source of land cover map: Landsat 8, Nasa 2016. Black lines in (b) show the flight tracks across the study areas in 2012 (solid) and 2013 (dashed).

For our study we chose two study areas, "North" and "South", (Fig. 1b-d), each about 1,000 km² large, in the northern and central part of the Mackenzie Delta. The waterbodies in both study areas are included in a high resolution permafrost waterbody database by Muster *et al*. (2017). In the study area "North", which is located north of the treeline in the outer delta, 17% of the area are covered with waterbodies. In the study area "South" in the central part of the delta 35% are covered with waterbodies, thus representing the pattern found in the entire delta (Mackay, 1963).

Methane flux data collection and analysis

We used CH_4 measurements from the Airborne Measurements of Methane Fluxes (AIRMETH) campaign (cf. Kohnert *et al*., 2014; Kohnert *et al*., 2017). AIRMETH aimed at assessing regional patterns of CH_4 fluxes across the arctic permafrost landscape of the Mackenzie Delta in Canada using the eddy-covariance (EC) technique. The study period was

from 4 July to 10 July 2012 (5 flight days, 44 flight tracks) and 19 July to 26 July 2013 (7 flight days, 40 flight tracks). We used the research aircraft Polar 5 of the Alfred Wegener Institute Helmholtz Centre for Polar and Marine Sciences (AWI) as platform for our measurements. For the flux measurements we flew 40 – 80 m above ground level to capture the exchange processes between the surface and the atmosphere with a true airspeed of 60 ms^{-1}. The height of the atmospheric boundary layer was determined based on vertical profile flights at the beginning and end of each flight track via changes in relative humidity and potential temperature. We excluded flights above the atmospheric boundary layer from this analysis. Wind speed and direction were obtained at 100 Hz from a Rosemount 5-hole probe attached to a 3 m nose boom mounted to the front of the airplane. Following Lenschow (1986) we derived the wind components u, v, and w with respect to the earth coordinate system. For the measurements of CH_4 wet mole fractions at 20 Hz, sample air was drawn from an inlet tube on top of the cabin into a gas analyser placed inside the cabin (in 2012: Fast Methane Analyzer FMA and in 2013: Fast Greenhouse Gas Analyser FGGA 24EP, both Los Gatos Research Inc., Mountain View, California, USA).

The flux data analysis was done in GNU R version 2.15, described in detail by Kohnert *et al.* (2017). In summary: The CH_4 data were first converted to dry mole fraction including spectroscopic correction after Tuzson (2010). High-resolution CH_4 fluxes were then calculated with a time-frequency-resolved version of the EC technique using the vertical wind speed and CH_4 dry mole fraction data (Metzger *et al.*, 2013; Metzger *et al.*, 2017). To reduce random uncertainty we aggregated these fluxes and derived an in-situ observed space-series of CH_4 fluxes between surface and atmosphere at a spatial resolution of 100 m. Using the footprint model of Kormann and Meixner (2001) the CH_4 fluxes were related to the associated surface. From the linear information along the flight tracks we obtained a map of the CH_4 fluxes within the combined area of all footprints at a 100 m x 100 m spatial resolution via flux

topographies (Mauder *et al*., 2008). We derived a standard error map for the flux map following Gatz and Smith (1995).

Classification of waterbody area based on TerraSAR-X data

For this study we used two waterbody maps from the circum-arctic database PeRL (Permafrost Region Pond and Lake) (Muster *et al*., 2017) (mdn00120100716 as our northern study area; mdw00120090921 as our southern study area). Both maps were produced based on TerraSAR-X data (Muster *et al*., 2017; North: data acquired at 16 July 2010; South: data acquired at 21 September 2009) and have a spatial resolution of 2.5 m. The data processing was done for both study areas in ESRI ArcMAP v10.4 and the data were projected to NAD83 UTM 8N. The CH_4 flux map and the waterbody maps were clipped to the mutual extent, leaving an area of 965 km² for the northern study area and 873 km² for the southern study area. For each grid cell of the CH_4 flux map, we calculated the fraction of water and land.

Classification of waterbody depth based on Sentinel-1 SAR data

Shallow waterbodies (< 2 m deep) can freeze through the entire depth during winter (cf. Marsh, 1991), forming so-called bedfast or grounded ice, whereas deeper waterbodies remain unfrozen beneath the ice cover. Synthetic Aperture Radar (SAR) data can be used to distinguish these two different waterbody ice regimes based on strong differences in the backscatter intensity signatures from grounded and floating ice (e.g. Jones *et al*., 2013; Antonova *et al*., 2016; Bartsch *et al*., 2017). The SAR signal penetrates through fresh ice and, in case of floating ice, scatters back from the rough ice bottom, resulting in high backscatter intensity. In case of grounded ice, the signal is absorbed into the waterbody bottom due to low

dielectric contrast between the ice and the frozen sediments, resulting in a low backscatter intensity.

For our study we exploited data from the SAR satellites Sentinel-1. The Sentinel-1 mission consists of two identical satellites, launched in 2014 and 2016, which image the entire Earth every six days. The SAR antennas operate in a C-band (frequency 5.405 GHz, wavelength 5.55 cm). The data is freely available at https://scihub.copernicus.eu/dhus/. We used two images which covered adjacent parts of the study region. Both images were acquired in Interferometric Wide Swath (IW) mode on 18 March 2015. The images are provided as a Ground Range Detected (GRD) product which contains the amplitude of the signal and is projected to the ground range using an Earth ellipsoid model with a cell size of 10 m x 10 m. The incidence angle ranged from 30° to 46° across both images. We chose the VV polarization from the available VH and VV polarizations, as the co-polarized SAR signal has a much stronger backscatter intensity and signal to noise ratio compared to the cross-polarization modes.

The data processing was performed in the ESA Sentinel-1 toolbox (S1TBX) embedded in the Sentinel Application Platform (SNAP). We improved the geocoding by using Range Doppler Terrain Correction with the 1 sec Global Digital Elevation Model (GDEM) from the ASTER (Advanced Spaceborne Thermal Emission and Reflection Radiometer) sensor. Backscatter intensity was calibrated to sigma nought values in decibels. The resulting backscatter intensity images were merged to a mosaic and reprojected to NAD83 UTM zone 8N.

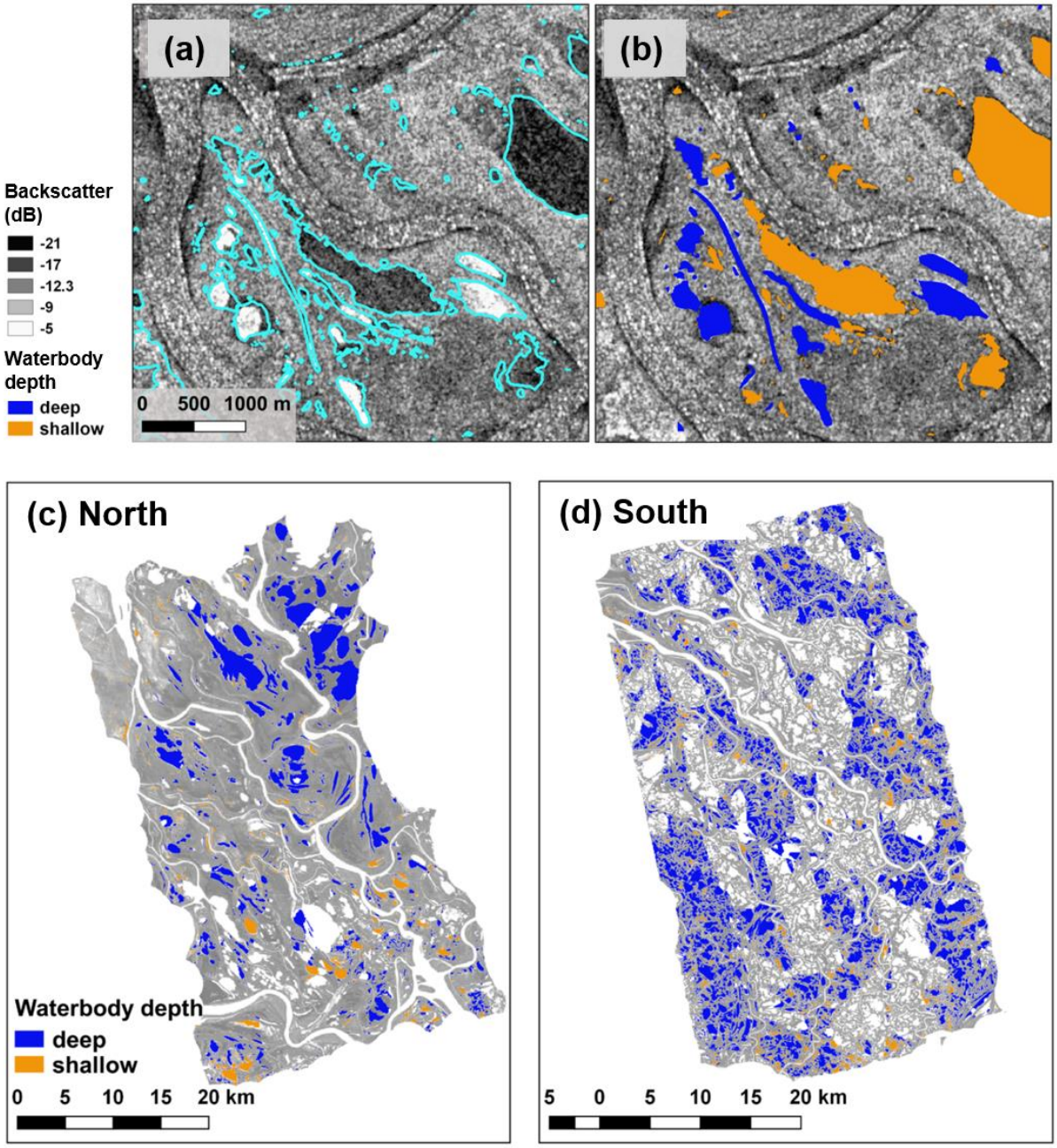

Fig. 2: Sentinel-1 backscatter intensity and waterbody depth classifications for the two study areas. (a) Sentinel-1 backscatter intensity image for a subset of the study area taken on 18.03.2015 in decibel. High backscatter intensity (bright areas on the waterbodies) correspond to floating ice, low backscatter intensity (dark areas on the waterbodies) correspond to grounded ice; (b) Waterbodies classified as "deep" (blue, approx.. > 2m deep) and "shallow" (orange, approx.. < 2 m deep) on the same subset as in (a); (c) and (d) distribution of shallow and deep waterbodies in (c) the study area "North" and (b) the study area "South". Note that only waterbodies with CH_4 measurements were included in the classification.

Waterbodies were extracted using the PeRL maps described in the previous chapter and only the subset of those waterbodies which were covered by CH_4 flux measurements were included in the further analysis. The backscatter intensity values were extracted for each waterbody containing ten or more Sentinel-1 pixels. To distinguish grounded and floating lake ice for all waterbodies within the entire mosaic we derived an empirical threshold. From the Sentinel-1

images, we visually identified 20 waterbodies with grounded and floating ice and sampled their backscatter intensity values. We determined the threshold as the average value of the two sample classes. As a result, all pixels with backscatter intensity values ≤ -12.3 dB were identified as grounded ice and all pixels with backscatter intensity values > -12.3 dB were identified as floating ice. For our analysis we classified a waterbody as "shallow" if ≥ 80 % of the ice pixels of a waterbody were grounded (orange in Fig. 2b-d) and "deep" if < 80% of the pixels were grounded (blue in Fig. 2b-d).

Manual coarsening of the resolution of the CH_4 fluxes

At the 100 m x 100 m grid cell size of the CH_4 flux map, a relation between waterbody characteristics and the CH_4 flux is not analyzable, as waterbodies larger than 100 m x 100 m and those that are not completely contained within one grid cell, are cut into fragments. This strong artificial fragmentation of waterbodies does not correspond to environmental processes. Moreover, larger grid cells of the CH_4 flux map are necessary to detect relationships between the number and type of waterbodies contained in the grid cells and the respective CH_4 fluxes. Therefore, we decreased the spatial resolution of the CH_4 flux map stepwise, to determine i) the relation between CH_4 flux and waterbody characteristics on a landscape scale and ii) the effect of different spatial resolutions on these relations.

For the analysis we first categorized the waterbodies based on their size, i.e.: large (> 10,000 m², i.e. larger than the resolution of the original CH_4 flux map and corresponding to the > 0.88 quantile (North) and > 0.78 percentile (South)), medium (≤ 10,000 m² and > 500 m²; between the 0.44 and 0.88 quantile (North) and 0.78 (South), respectively) and small (≤ 500 m²; < 0.44 quantile (North and South), and their depth, namely "deep" and "shallow". Secondly, we decreased the resolution of the CH_4 flux map stepwise (500 m,

1,000 m, 2,500 m, 5,000 m, and 10,000 m). To determine information loss and changes in spatial patterns, we resampled the previously coarsened CH_4 flux maps back to a resolution of 100 m. We then calculated the relative changes between these resampled flux maps compared to the original 100 m flux map. For each manually coarsened spatial resolution we calculated the number of waterbody centroids per grid cell to avoid double-counting of waterbodies that cover several grid cells. We then calculated the zonal statistics for each grid cell to relate the waterbody information to the CH_4 flux.

Comparing Mackenzie Delta fluxes and literature-reported fluxes from Arctic ecosystems

Lastly, we compared the CH_4 emissions from our study areas, which are integrated across land cover classes, to literature-reported fluxes from northern ecosystems by scaling the latter to the extent of our study areas. We based the scaling on the PeRL waterbody maps (Muster *et al*., 2017) and on the waterbody classes and corresponding CH_4 fluxes reported in a review study by Wik *et al*. (2016b). We allocated the CH_4 fluxes from their category "peatland ponds" ($\leq 10^5$ m²) to the class "ponds", and the mean CH_4 flux of their categories glacial/post-glacial lakes and thermokarst lakes ($> 10^5$ m^2) to the class "lakes". The tundra CH_4 fluxes were based on the mean flux reported by several studies (Sachs *et al*., 2008, Wille *et al*., 2008, O'Shea *et al*., 2014, and Heikinnen *et al*., 2002). The underlying areal extent of the land, pond, and lakes class for each study area is provided in table 1. The exemplary CH_4 emissions were calculated in a back-of-an-envelope calculation for the growing season and zero curtain period with soil temperatures around 0°C of the year 2013. For the Mackenzie Delta this period was 165 days in 2013 based on North American Regional Reanalysis (NARR) data (Mesinger *et al*., 2006) for soil temperature in 10 cm depth. It should be noted that the airborne CH_4 measurements were conducted during peak growing season, whereas

the literature data originate from different times during the growing season. This might lead to a slight overestimation of the airborne CH_4 emissions throughout the growing season.

Table 1: Share of land cover classes per study area with ponds defined as < 10^5 m² and lakes defined as > 10^5 m².

	Total area	**Area land**	**Area ponds**	**Area lakes**
Study area "North"	969.48 km²	805.43 km²	26.18 km²	137.87 km²
Study area "South"	877.81 km²	569.48 km²	65.08 km²	243.25 km²

Results

CH_4 emission and waterbody properties in the study areas

The median CH_4 emission in the northern study area was 2.43 mg m^{-2} h^{-1} and the median CH_4 emission in the southern study area was 1.32 mg m^{-2} h^{-1}, with the northern area featuring distinct hot spot areas of emissions (Fig. 3, 4a). CH_4 fluxes directed from the surface towards the atmosphere are defined as positive, fluxes towards the surface as negative.

The northern study area contained less waterbodies (n = 6,784) than the southern area (n = 10,273). The majority of waterbodies in the north were between 10^2 m^2 and 10^5 m^2 in size (median 624 m²) and it also included the largest ones (up to 1.54 x 10^7 m^2) (Fig. 4b), while in the southern study area, the waterbodies were more equally distributed between 2.5 m² and 10^6 m^2 (median 779 m^2) with a maximum size of 7.2 x 10^6 m^2. In absolute numbers, the northern area was dominated by shallow waterbodies, while deeper waterbodies characterized the southern area (Fig. 5). However, in terms of area fractions, 17 % of all waterbodies in the northern study area were shallow versus only 8.2 % in the southern area. In both study areas, the area distributions of shallow and deep waterbodies strongly overlapped (Fig. 6). Especially in the northern study area, the numbers of shallow and deep waterbodies

peaked at the same range of waterbody sizes (Fig. 6). Within and between both study areas the spatial distributions of waterbodies and waterbody types were heterogeneous (Fig. 7).

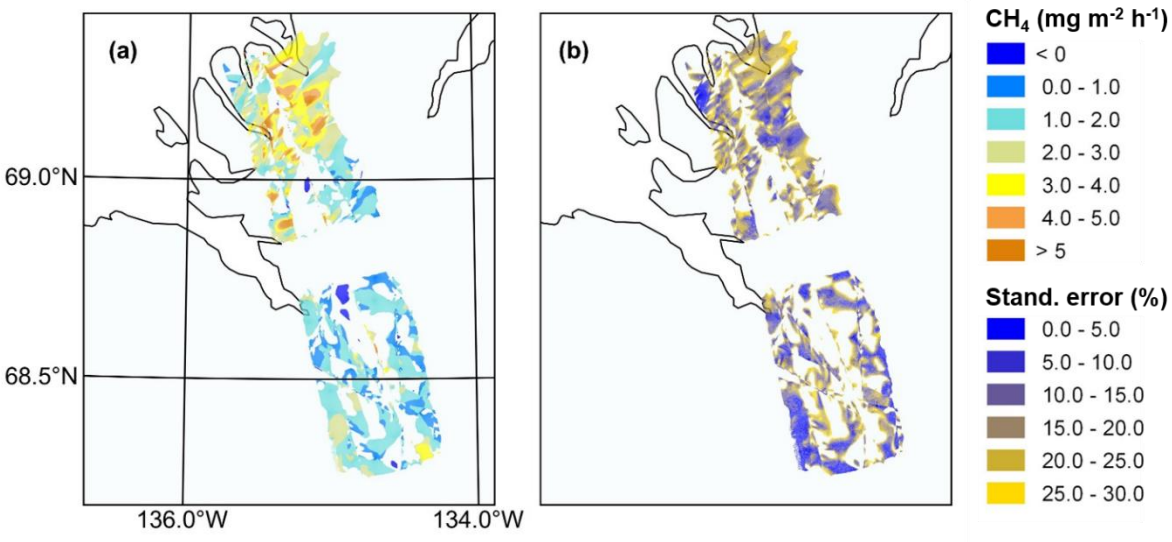

Fig. 3: (a) Spatial patterns of the CH_4 fluxes across the final extent of the study areas after excluding areas without CH_4 measurements or without available waterbody information. (b) Standard error of the remaining CH_4 fluxes.

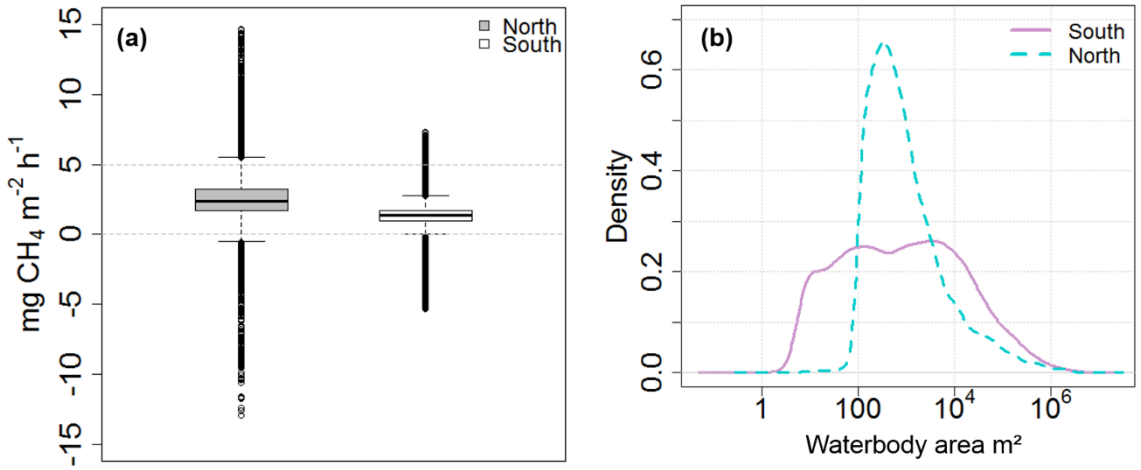

Fig. 4: (a) Distribution of the CH_4 fluxes in the two study areas. (b) Distribution of waterbody areas for the northern (10,273 waterbodies) and southern (6,784 waterbodies) study area. The x-axis is on a log-scale.

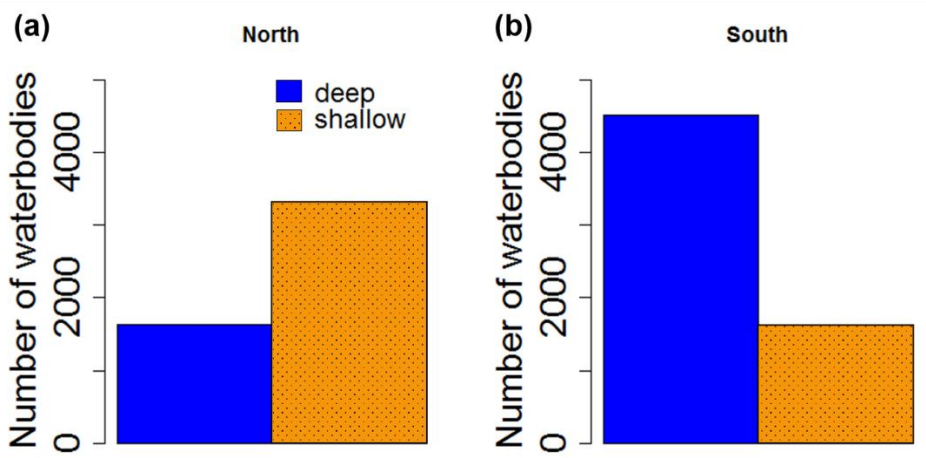

Fig. 5: Number of deep (> 2 m deep) and shallow (< 2 m deep) waterbodies in (a) the study area "North" and (b) the study area "South".

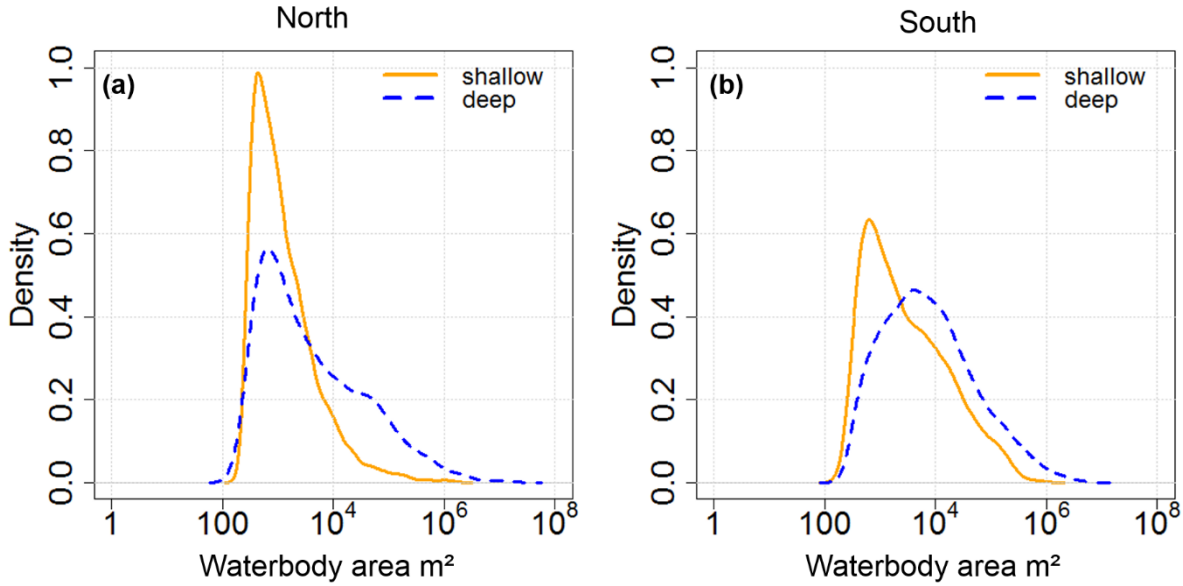

Fig. 6: Density plots of waterbody area for shallow and deep waterbodies in the (a) northern (10,273 waterbodies) and (b) southern (6,784 waterbodies) study area.

Spatial patterns and information loss of CH_4 fluxes at different resolutions

To determine a spatial resolution of the CH_4 flux that causes little information loss while allowing to reduce fragmentation of waterbodies, we first analyzed the changes in the median CH_4 fluxes at coarser resolutions. Due to strong emission hot spots in the northern study area that were averaged out during the resampling, the CH_4 flux at the original 100 m resolution and the resampled resolutions were significantly different. However, the median fluxes only

decreased from 2.43 mg m^{-2} h^{-1} (at 100 m resolution) to 1.94 mg m^{-2} h^{-1} (at 10,000 m resolution). In the southern study area the fluxes did not change significantly with a median flux of 1.32 mg m^{-2} h^{-1} at 100 m resolution and resampled fluxes ranging between 1.32 mg m^{-2} h^{-1} (5,000 m resolution) and 1.4 mg m^{-2} h^{-1} (10,000 m resolution). Between the coarsened resolutions alone, the median CH_4 flux did, however, not change significantly ($\alpha = 0.05$; Kruskal-Wallis rank sum test, north: $p = 0.15$, south: $p = 0.82$). The spatial patterns of the CH_4 fluxes (Fig. 8a and Fig. 8c) were best preserved at the resolutions of 500 m and 1,000 m in both study areas.

The relative changes between the original 100 m x 100 m flux map and the resampled flux maps at different resolutions are shown in Fig. 8b and Fig. 8d. In both study areas, the 0.99 quantile of the absolute values of the relative changes was < 1 for the resolutions 500 and 1000, but > 1 for the coarser resolutions. Based on that we considered the information loss for the two higher resolutions acceptable.

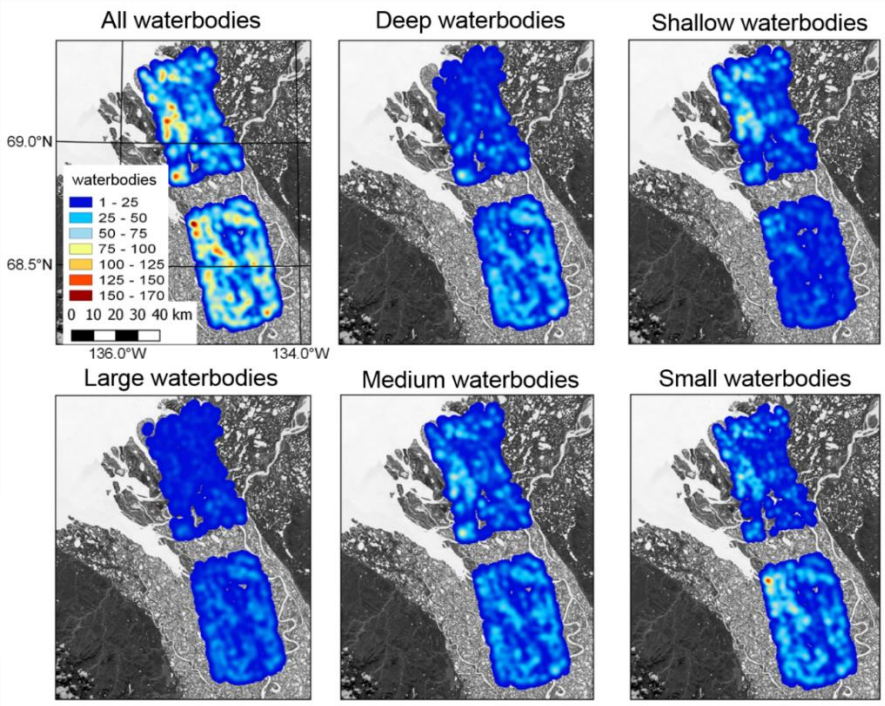

Fig. 7: Spatial distribution of waterbody types in the two study areas. The values represent the amount of waterbodies within the grid cell of 2,500 m x 2,500 m. The waterbodies were classified as follows: "Large waterbodies" (> 10,000 m²), "medium waterbodies" (500 - 10,000 m²), "small waterbodies" (< 500 m²). The maps were produced in QGIS 2.18.4 ('heatmap plugin'; settings: Kernel shape: Quartic biweight, radius 2,500 m, cell size 100 m).

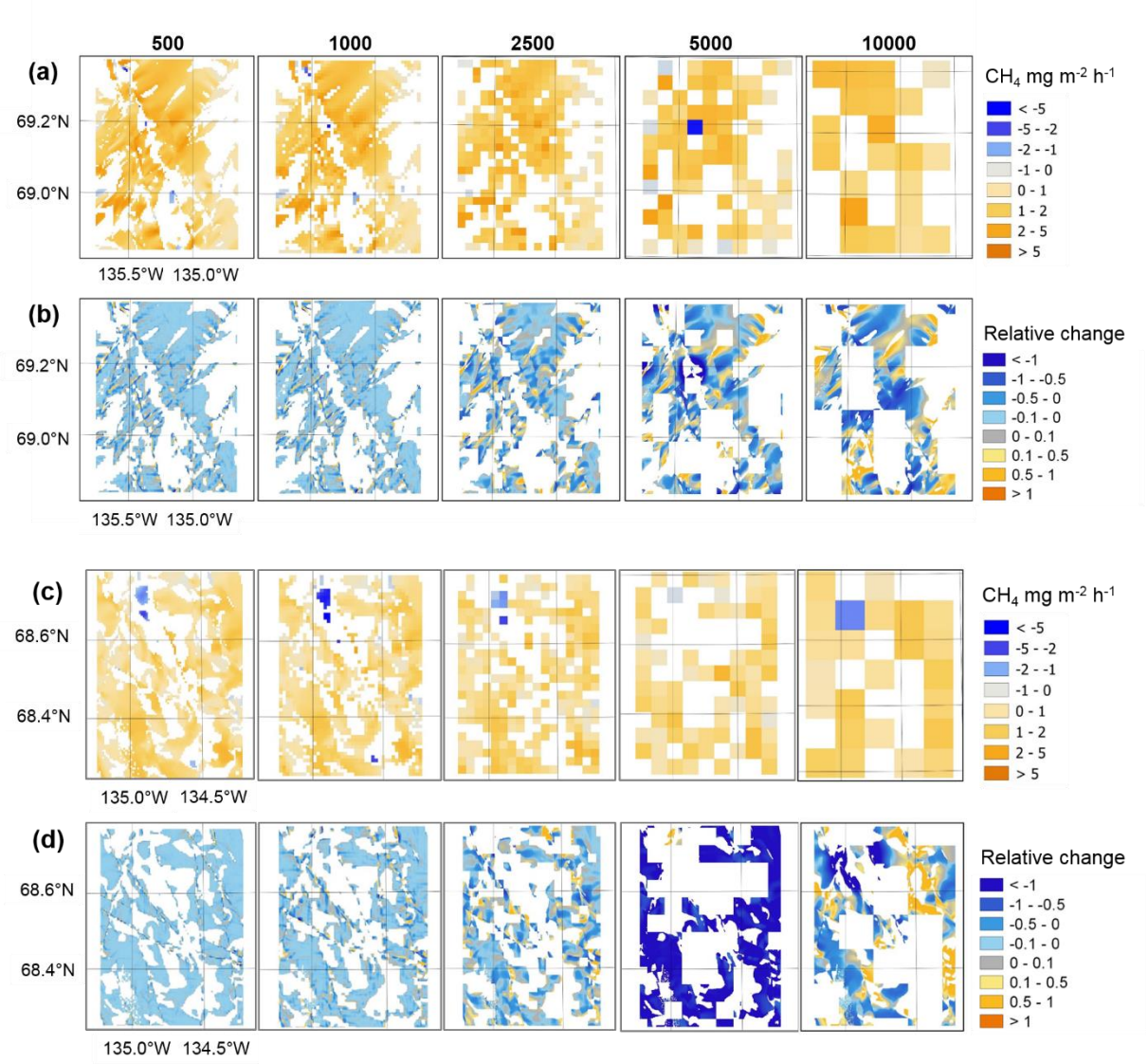

Fig. 8: Study area "North": (a) CH_4 flux resampled for different spatial resolutions in m (numbers above subplots in m). (b) Relative changes between the original 100 m CH_4 flux map and the resampled flux maps at the different resolutions. Positive values represent cases in which the original flux was smaller than the resampled flux, and negative values represent the opposite case. Study area "South": (c) CH_4 flux and (d) relative changes as described for "North".

Do CH_4 emissions from waterbodies exceed those from the surrounding land surface?

We compared the CH_4 fluxes at a resolution of 100 m for grid cells covered only by land and only by water within our two study areas (Fig. 9). Within each study area the median fluxes above land (North: 2.36 mg m^{-2} h^{-1}; South: 1.34 mg m^{-2} h^{-1}) and water (North: 2.34 mg m^{-2} h^{-1}; South: 1.34 mg m^{-2} h^{-1}) were similar. However, in the northern study area, the entirety of CH_4 fluxes from land surface, including the extremely large fluxes, were significantly higher (Wilcoxon-Rank-Sum-Test: $p = 0.02$, $\alpha = 0.05$) compared to fluxes from

water surface. In contrast, in the southern study area there was no significant difference between the two classes for the entirety of the fluxes (Wilcoxon-Rank-Sum-Test, $p = 0.46$, $\alpha = 0.05$). At coarser resolutions we analyzed the percentage of a grid cell covered with water in relation to the CH_4 flux. In the northern study area (Fig. 10a) the CH_4 flux was weakly negatively (cor = -0.05) correlated to the water coverage at a 500 m resolution, whereas there was no significant correlation at coarser resolutions. In the southern study area the CH_4 flux was not correlated significantly with water coverage (Fig. 10b).

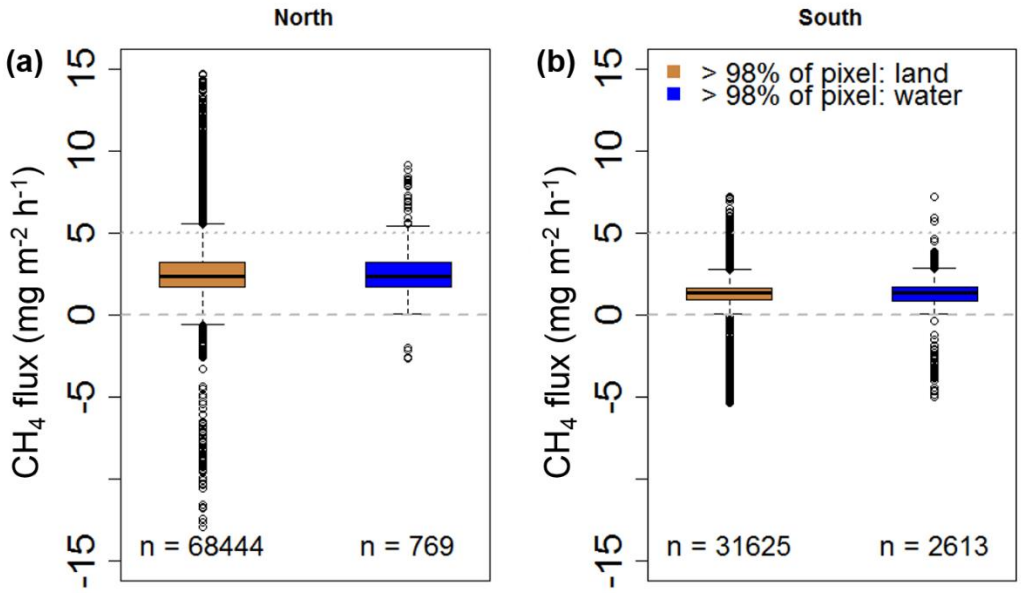

Fig. 9: CH_4 flux per land cover class land (> 98% of grid cell are land) and water (>98% of grid cell is water) based on grid cell size of 100 m for (a) the northern and (b) the southern study area.

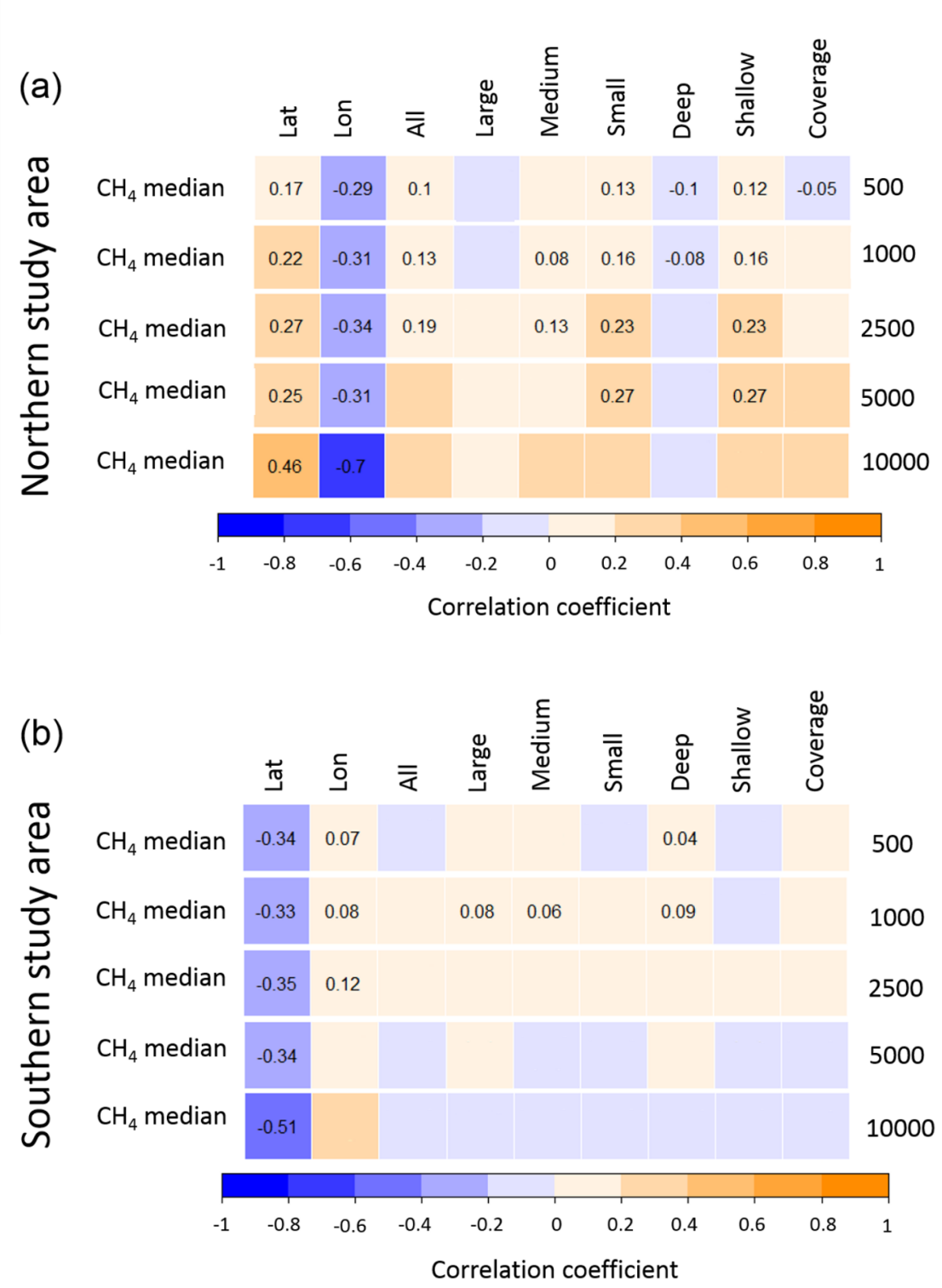

Fig. 10: Correlations between median CH_4 fluxes and coordinates and numbers of waterbodies of different waterbody characteristics (size and depth) at different resolutions for (a) the northern and (b) the southern study area. The values in the boxes are the respective correlation coefficients. Orange colors show positive correlations. Blue colors show negative correlations. Boxes without correlations coefficients show cases in which the correlations were not significant.

Relations between waterbody characteristics and CH_4 flux across different resolutions

There was no strong correlation between waterbody characteristics and CH_4 flux in either study area at any resolution (Fig. 10). In the northern study area, the correlations that existed between waterbody properties and the CH_4 flux were weakly positive, except for the number of deep waterbodies which was weakly negatively correlated (Fig. 10a). In contrast, stronger positive correlations existed between latitude and CH_4 flux and stronger negative correlations between longitude and CH_4 flux. In the southern study area, even fewer weak correlations could be detected (Fig. 10b). In contrast to the northern study area, the number of deep waterbodies was weakly positively correlated with the CH_4 flux. Latitude was stronger negatively correlated with CH_4 flux, while longitude was only weakly positively correlated. While in the northern study area a higher number of all, small or shallow waterbodies was correlated with a higher CH_4 flux, this was surprisingly not the case in the southern study area. Moreover, in both study areas, weak correlations that existed for the higher resolutions did not exist in coarser resolutions of the CH_4 flux.

How do the Mackenzie Delta CH_4 fluxes compare to fluxes reported from the circum-Arctic?

For both study areas, the CH_4 emissions per warm season calculated based on literature values differed from those derived from the airborne measurements (Table 2). The literature estimates reproduced the northern study area's larger emission compared to the southern study area, originating from the slightly larger extent, as the emissions per square kilometer did not differ (0.006 Gg per square kilometer). Instead, major differences were found between the estimates derived from literature and airborne EC fluxes. While for the northern study area the literature-based emission estimate accounted for only 62 % of the measured emissions, for the southern study area the literature-based CH_4 emission estimate was similar to that derived from airborne EC data (105 %). Even when calculating the emissions of the northern study

area based on the median CH_4 flux derived from AIRMETH excluding potential strong geologic CH_4 fluxes > 5 mg m^{-2} h^{-1} that Kohnert *et al*. (2017) found in the northern study area, the emission based on literature values would still only be 64 % of the emission from AIRMETH data (8.99 Gg).

Table 2: Comparison of CH_4 emissions for the two study areas "North" and "South" based on our measured fluxes and based on literature flux values extrapolated with highly resolved land cover classes (land, ponds and lakes).

Name	**Land**	**Ponds*** <= 10^5 m²	**Lakes**** > 10^5 m²	**Gg per warm season 165 d*****
Literature "North"	1.65 mg m^{-2} h^{-1}	2.74 mg m^{-2} h^{-1}	0.42 mg m^{-2} h^{-1}	5.78
Literature "South"				4.83
AIRMETH "North"	Median flux in study area: 2.432 mg m^{-2} h^{-1} ****			9.34
AIRMETH "South"	Median flux in study area: 1.323 mg m^{-2} h^{-1} ****			4.6

* Ponds: Wik *et al*., 2016b: peatland ponds: 65.9 mg m^{-2} d^{-1}

** Lakes: Wik *et al*., 2016b: glacial/post-glacial + thermokarst lakes (mean flux value): (7.5 + 12.7)/2 = 10.1 mg m^{-2} d^{-1}

*** Warm season: growing season plus zero curtain period, when soil temperatures are around 0°C. Based on North American Regional Reanalysis (NARR) data (Mesinger *et al*., 2006) for soil temperature in 10 cm depth this was the case on 165 days of the year.

**** including geologic CH_4 emission (Kohnert *et al*., 2017)

Discussion

Comparison of CH_4 fluxes from water vs land

The comparison between CH_4 fluxes from land and water surface unveiled differences between the northern and southern study area. In the northern study area, land surface fluxes exceeded those from water and a higher coverage with waterbodies was actually negatively correlated with the CH_4 flux. This finding alone could be attributed to the existence of strong geologic CH_4 emissions from land surface that Kohnert *et al.* (2017) identified mainly in the northern study area. However, also in the southern study area the emissions from waterbodies

did not exceed those from land surface, even though there are hardly any geologic CH_4 emission hot spots (Fig. 9).

Our results suggest that CH_4 emissions from waterbodies do not generally exceed those from the surrounding land surface. Although the measurements only represent snapshots during the most productive period of a year, we assume that our data include spontaneously occurring ebullition events (Sabrekov *et al*., 2017; Walter Anthony *et al*., 2006) and other temporal emission peaks. Peak emissions from waterbodies seem to have been too weak to be visible or influential on a regional scale. On an annual scale, temporal variability of CH_4 emissions from waterbodies might be introduced by potential CH_4 outbursts during the ice breakup in spring or potential autumn turnover in some waterbodies (López Bellido *et al*., 2009; Phelps *et al*., 1998). These two processes can transform waterbodies into temporal CH_4 emission hotspots and were not reflected in our measurements. Additionally, the margins of waterbodies are considered especially strong emitters of CH_4 (Walter Anthony *et al*., 2016), but our study suggests that they may not be able to tip the balance on a larger spatial scale.

Correlations of waterbody characteristics and CH_4 fluxes

In this chapter we discuss the relations between waterbody characteristics and CH_4 flux found for the higher resolutions (500 m and 1,000 m) as more reliable due to only little information loss compared to the original resolution. Nonetheless, we would like to point out that at coarser resolutions the correlations between CH_4 flux and waterbody types in some cases changed regarding direction, intensity or significance. For instance, at a resolution of 10,000 m no significant correlations were detected, indicating that conclusions merely based on this data would be misled.

For the two higher resolutions, it is striking that we did not detect a general pattern in the relations between the waterbody characteristics and the CH_4 flux that would be valid in the northern and southern study area in either resolution. This shows that even within a region like the Mackenzie Delta, correlation patterns are not necessarily transferable from one subregion to another. Part of the inconsistent correlations could be caused by the current spatial resolution of the CH_4 flux map, which does not resolve waterbodies smaller than 100 m individually causing a "mixed pixel" effect. Additionally, the differences in the correlations in the two study areas could be caused by differences in the ecology or structure of the landscapes, even though the study areas are only located about 20 km apart. While the northern study area is a tundra ecosystem which is characterized by strong CH_4 emissions caused partly by geologic CH_4 sources, the southern study area resembles a taiga ecosystem. Nonetheless, and even despite the different waterbody type distributions in the two study areas, generally valid correlations should have been detectable, if waterbodies had a strong influence on CH_4 emission on a regional scale. We found, however, for both study areas, only very weak correlations between waterbodies and the CH_4 flux (North: correlation coefficients < 0.2; South: correlation coefficients < 0.1). Especially in the southern study area, only few significant correlations existed.

These weak correlations do, however, shed light on the contribution of small and shallow waterbodies to regional CH_4 emissions. Our results suggest that areas with a large number of shallow or small lakes are not generally characterized by higher CH_4 emissions. While in the northern study area the number of small or shallow waterbodies was in fact weakly correlated with the CH_4 flux, this was not the case in the southern study area. This suggests that shallow and small waterbodies only in some cases act as strong CH_4 sources (Sabrekov *et al*., 2017; Wik *et al*., 2016b; Holgerson & Raymond, 2016; Langer *et al*., 2015) that are visible on a regional scale. Overall, the weak correlations and missing general correlation patterns indicate

that on a regional scale waterbodies in general or waterbody types as defined here do not act as major CH_4 emission hotspots in either study area, but that latitude and longitude, that are substituting e.g. temperature, productivity, or vegetation, have a stronger influence on patterns of CH_4 fluxes. Additionally, regional patterns in CH_4 emissions from arctic waterbodies can be caused by differences in nutrient status or colored dissolved organic matter content (Rasilo *et al*., 2015).

In the future, consequences of climate change might, however, alter the role of waterbodies in the CH_4 budget of the Mackenzie Delta. For northern Alaska Arp *et al*. (2016) showed that the temperatures of shallow lakes have already increased substantially over the last three decades leading to fast thaw of permafrost below shallow waterbodies. Additionally, the high number of through-taliks below waterbodies in the Mackenzie Delta (Ensom *et al*., 2012) could increase and form connections to deeper CH_4 sources. Marsh (1991) showed for the Mackenzie Delta that ice thickness is sensitive to snow depth and snow density. For the shallow waterbodies in the Mackenzie Delta even small changes in the snow characteristics could have an effect on whether a waterbody freezes to the bottom and thus whether or not it enables year-round CH_4 production. These changes could increase the importance of CH_4 emissions from waterbodies in the Mackenzie Delta on a regional scale. To continue the assessment of the contribution of waterbodies to the CH_4 flux on a regional scale, it is necessary to establish a characterization of waterbodies that can be used independently of study area and spatial resolution. The highly resolved TerraSAR-X and Sentinel-1 data provide a promising basis as they allow for distinguishing more precisely between wetlands and waterbodies. Additional work is warranted to approach this spatial granularity and level of detail also with the CH_4 emission observations: while the spatial resolution of the current emission map is 100 m, waterbodies with smaller length scales dominate the size distributions in both study areas (Fig. 4). The resulting “mixed pixel” effect could be mitigated by

determining the CH_4 emissions on a per-waterbody basis: One option would be to increase the spatial resolution of measurements by flying closer to the ground, e.g. by profiting from technical advances in drones. Alternatively, the flux map creation algorithm could target individual (pure) vector objects such as waterbodies rather than regular (mixed) grid cells. Both would pave the way towards attributing CH_4 fluxes derived from airborne measurements to single waterbodies and would enable us to detect differences between waterbodies within a region.

How do the Mackenzie Delta CH_4 fluxes compare to fluxes reported from the circum-Arctic?

The Mackenzie Delta is the second largest arctic delta (Burn & Kokelj, 2009) and contains a large number of waterbodies (Emmerton *et al*., 2007). Our two study areas cover a taiga ecosystem and a tundra ecosystem located in an outer river delta with geologic CH_4 sources (Bowen *et al*., 2008) and therewith provide an interesting contrast to study the regional role of CH_4 emissions from waterbodies. For both study areas the mean waterbody areas belong in the larger half of the 30 study sites that were mapped at high spatial resolution for the permafrost waterbody database developed by Muster *et al*. (2017) and that are distributed across the Arctic. However, both study areas themselves and in comparison are characterized by the spatial heterogeneity of waterbody distribution described above. Our airborne measurements cover the entire areas at high resolution and include all CH_4 sources within these areas. We thus cover a large variety of waterbody types, including small waterbodies that may locally act as strong CH_4 sources and avoid biased sampling on a waterbody scale that had been identified by Wik *et al*. (2016a) as a source for underestimating CH_4 fluxes from waterbodies.

The differences between the study areas are also reflected in the landscape scale CH_4 emissions, which differ strongly between the two regions when based on the airborne EC

data. This difference is not reflected in the estimates based on literature biogenic fluxes. The differences between literature and airborne EC emissions are especially large in the northern study area, where Kohnert *et al.* (2017) detected strong emissions from geologic CH_4 sources belowground in addition to extensive biogenic CH_4 emissions. In contrast, in the southern study area the discrepancy between the measured and calculated landscape emissions is low. Assuming that the approximation based on the literature values should work comparably well in the northern study area given the use of the same data sets, the discrepancy could point out the large contribution of geologic CH_4 emissions to this region's CH_4 budget (Kohnert *et al.*, 2017). In this area, the geologic emissions seem to not only originate from hot spots, but weaker geologic CH_4 emissions could be spread out across large portions of the study area in addition to the microbial CH_4 emissions. Thus, geologic emissions could be contributing to about 40 % of the northern study area's CH_4 emission.

It is striking, that for both study areas the literature based bottom-up estimates almost reflect or underestimate the measured CH_4 emissions, as bottom-up estimates are generally thought to overestimate landscape scale emissions (Thornton *et al.*, 2016). That might indicate that overall CH_4 emissions from a common area such as the southern study site – at least in some cases – can be approximated using average literature flux values, if they are combined with a very high-resolution land cover map. For a circum-Arctic extent, however, available land cover information has been too coarse and CH_4 data too scarce or too coarse.

Overall, waterbodies could not be detected to be such strong CH_4 sources that would enhance the CH_4 emission on a regional scale, although the numbers of some waterbody types are weakly correlated with the CH_4 flux. For the future it will be interesting to see if a warmer climate leads to such a strong increase in CH_4 emissions from permafrost waterbodies, that they become distinguishable as hot spots even on a regional scale. For this it is crucial to

improve our understanding of waterbody properties that reflect waterbodies across different regions and areal extents.

Author contribution

K.K. and S. Muster initialized the study as part of the AIRMETH campaigns that were designed and guided by T.S. and J.H. CH_4 data were collected by K.K, A.S., J.H. and T.S. collected the CH_4 data. S. Muster classified the lakes based on TerraSAR-X data. B.J. prepared the Sentinel-1 data. S.A. and B.J. did the interpretation of the Sentinel-1 backscatter signals. J.H. processed the raw aircraft data. A.S. and S. Metzger contributed to the CH_4 flux calculations. K.K. lead the analysis with inputs from all authors. K.K. wrote the manuscript with inputs from all authors.

Competing interests

The authors declare that they have no conflict of interest.

Acknowledgements

This work was supported by the Helmholtz Association of German Research Centres through a Helmholtz Young Investigators Group grant to T.S. (grant VH-NG-821) and is a contribution to the Helmholtz Climate Initiative REKLIM (Regional Climate Change). Work of Sina M. was supported by the Helmholtz Association through grant VH-NG 203. We thank Stephan Lange for his support with the lake data analysis. The National Ecological Observatory Network is a project sponsored by the National Science Foundation and managed under cooperative agreement by Battelle Ecology, Inc. This material is based upon work supported by the National Science Foundation [grant DBI-0752017]. Any opinions, findings, and conclusions or recommendations expressed in this material are those of the author and do not necessarily reflect the views of the National Science Foundation. The AIRMETH

campaigns were mainly funded by Alfred Wegener Institute Helmholtz Centre Helmholtz Centre for Polar and Marine Research, Bremerhaven, Germany.

References

Antonova S, Duguay, CR, Kääb A, Heim B, Langer M, Westermann S, Boike J (2016) Monitoring Bedfast Ice and Ice Phenology in Lakes of the Lena River Delta Using TerraSAR-X Backscatter and Coherence Time Series. *Remote Sensing*, **8**, 903.

Arp CD, Jones BM, Grosse G, Bondurant AC, Romanovsky VW, Hinkel KM, Parsekian AD (2016) Threshold sensitivity of shallow Arctic lakes and sublake permafrost to changing winter climate. *Geophysical Research Letters*, **43**, 6358-6365.

Bartsch A, Pointner G, Leibmann MO, Dvornikov YA, Khomutov AV, Trofaier AM (2017) Circumpolar Mapping of Ground-Fast Lake Ice. *Frontiers in Earth Science*, **5**, 12.

Bastviken D, Cole J, Pace M, Tranvik L (2002) Methane emissions from lakes: Dependence of lake characteristics, two regional assessments, and a global estimate. *Global Biogeochemical Cycles*, **18**, GB4009.

Bastviken D, Cole J, Pace M, Tranvik L (2004) Methane emissions from lakes: Dependence of lake characteristics, two regional assessments, and a global estimate. *Global Biogeochemical Cycles*, **18**, GB4009.

Bowen RG, Dallimore SR, Côte MM, Wrigth JF, Lorenson TD (2008) Geomorphology and gas release from pockmark features in the Mackenzie Delta, Northwest Territories, Canada. In Kane DL, Hinkel KM (Eds). *Proceedings of Ninth International Conference on Permafrost* (pp. 171-176). Fairbanks, Alaska: Institute of Northern Engineering.

Burn CR (2002) Tundra lakes and permafrost, Richards Island, western Arctic coast, Canada. *Canadian Journal of Earth Sciences*, **39**, 912-925.

Burn CR, Kokelj SV (2009) The Environment and Permafrost of the Mackenzie Delta Area. *Permafrost and Periglacial Processes*, **20**, 83-105.

Carson MA, Conly FM, Jasper JN (1999) Riverine sediment balance of the Mackenzie Delta, Northwest Territories, Canada. *Hydrological Processes*, **13**, 2499-2518.

Dlugokencky E, Nisbet EG, Fisher R, Lowry D (2011) Global atmospheric methane: budget, changes and dangers. *Philosophical Transactions of the Royal Society*, **369**, 2058-2072.

Emmerton CA, Lesack LFW, Marsh P (2007) Lake abundance, potential water storage, and habitat distribution in the Mackenzie River Delta, western Canadian Arctic. *Water Resources Research*, **43**, W05419.

Ensom TP, Burn CR, Kokelj SV (2012) Lake- and channel-bottom temperatures in the Mackenzie Delta, Northwest Territories. *Canadian Journal of Earth Sciences*, **49**, 963-978.

Heikinnen JEP, Maljanen M, Aurela M, Hargreaves KJ, Martikainen PJ (2002) Carbon dioxide and methane dynamics in a sub-Arctic peatland in northern Finland. *Polar Research*, **21**, 49-62.

Gatz DF, Smith L (1995) The standard error of a weighted mean concentration – I. Bootstrapping vs other methods. *Atmospheric Environment*, **29**, 1185-1193.

Holgerson MA, Raymond PA (2016) Large contribution to inland water CO_2 and CH_4 emissions from very small ponds. *Nature Geoscience*, **9**, 222-229.

Hugelius G, Strauss J, Zubrzycki S, Harden JW, Schuur EAG, Ping C-L, Schirrmeister L, Grosse G, Michaelson GJ, Koven CD, O'Donnell JA, Elberling B, Mishra U, Camill P, Yu Z,

Palmtag J, Kuhry P (2014) Estimated stocks of circumpolar permafrost carbon with quantified uncertainty ranges and identified data gaps. *Biogeosciences*, **11**, 6573-6593.

Jakobsson M, Andreassen K, Bjarnadóttir LR, Dove D, Dowdeswell JA, England JH, Funder S, Hogan K, Ingólfsson Ó, Jennings A, Larsen NK, Kirchner N, Landvik JY, Mayer L, Mikkelsen N, Möller P, Niessen F, Nilsson J, O'Regan M, Polyak L, Nørgaard-Pedersen N, Stein R (2014) Arctic Ocean glacial history. *Quaternary Science Reviews*, **92**, 40-67.

Jones BM, Gusmeroli A, Arp CD, Strozzi T, Grosse G, Gaglioti BV, Whitman MS (2013) Classification of freshwater ice conditions on the Alaskan Arctic Coastal Plain using ground penetrating radar and TerraSAR-X satellite data. *International Journal of Remote Sensing*, **34**, 8267-8279.

Kohnert K, Serafimovich A, Hartmann J, Sachs T (2014) Airborne Measurements of Methane Fluxes in Alaskan and Canadian Tundra with the Research Aircraft „Polar 5". *Reports on Polar and Marine Research*, **673**. ISSN:1866-3192.

Kohnert K, Serafimovich A, Metzger S, Hartmann J, Sachs T (2017) Strong geologic methane emissions from discontinuous terrestrial permafrost in the Mackenzie Delta, Canada. *Scientific Reports*, **7**, 5828.

Kormann R, Meixner, FX (2001) An analytical footprint model for non-neutral stratification. *Boundary-Layer Meteorology*, **99**, 207-224.

Langer M, Westermann S, Walter Anthony K, Wischnewski K, Boike J (2015) Frozen ponds: production and storage of methane during the Arctic winter in a lowland tundra landscape in northern Siberia, Lena River delta. *Biogeosciences*, **12**, 977-990.

Laurion I, Vincent WF, MacIntyre S, Retamal L, Dupont C, Francus P, Pienitz R (2010) Variability in greenhouse gas emissions from permafrost thaw ponds. *Limnology and Oceanography*, **55**, 115-133.

Lehner B, Döll, P (2004) Development and validation of a global database of lakes, reservoirs, and impoundments. *Journal of Hydrology*, **269**, 1-22.

Lenschow DH (1986) *Probing the Atmospheric Boundary Layer*. Boston, Massachusetts, American Meteorological Society.

López Bellido J, Tulonen T, Kankaala P, Ojala A (2009) CO2 and CH4 fluxes during spring and autumn mixing periods in a boreal lake (Pääjärvi, southern Finland). *Journal of Geophysical Research*, **114**, G04007.

Mackay JR (1963) *The Mackenzie Delta Area, N.W.T.* Ottawa, Ontario: Memoir 8. Geographical Branch, Department of Mines and Technical Surveys.

Marsh P (1991) Evaporation and ice growth in Mackenzie Delta lakes. In Schiller G, Lemmela R, Spreafico M (Eds) *Hydrology of Natural and Manmade Lakes*. Proceedings of the Vienna Symposium 1991. Wallingford, Oxfordshire, International Association of Hydrological Sciences.

Mauder M, Desjardins RL, MacPherson I (2008) Creating Surface Flux Maps From Airborne Measurements: Application to the Mackenzie Area GEWEX Study MAGS 1999. *Boundary-Layer Meteorology*, **129**, 431-450.

McGuire AD, Anderson LG, Christensen TR, Dallimore S, Guo L, Hayes DL, Heimann M, Lorenson TD, Macdonald RW, Roulet N (2009) Sensitivity of the carbon cycle in the Arctic to climate change. *Ecological Monographs*, **79**, 523-555.

Melton JR, Wania R, Hodson EL *et al*. (2013) Present state of global wetland extent and wetland methane modelling: conclusions from a model inter-comparison project (WETCHIMP). *Biogeosciences*, **10**, 753-788.

Mesinger F, DiMego G, Kalnay E *et al*. (2006). North American Regional Reanalysis. *Bulletin of the American Meteorological Society*, **87**, 343-360.

Metzger S, Durden D, Sturtevant C *et al*. (2017) eddy4R: A community-extensible processing, analysis and modeling framework for eddy-covariance data based on R, Git, Docker and HDF5. *Geoscientific Model Development*, **10**, 3189-3206.

Metzger S, Junkermann W, Mauder M, Butterbach-Bahl K, Trancón y Widemann B, Neidl F, Schäfer K, Wieneke S, Zheng XH, Schmid HP, Foken T (2013) Spatially explicit regionalization of airborne flux measurements using environmental response functions. *Biogeosciences*, **10**, 2193-2217.

Muster S, Roth K, Langer M, *et al*. (2017) PeRL: A circum-Arctic Permafrost Region Pond and Lake Database. *Earth System Science Data*, **9**, 317-348.

Natchimuthu S, Sundgren I, Gålfalk M, Klemedtsson L, Crill P, Danielsson Å, Bastviken D (2015) Spatio-temporal variability of lake CH_4 fluxes and its influence on annual whole lake emission estimates. *Limnology and Oceanography*, **61**, S13-S26.

O'Shea SJ, Allen G, Gallagher MW *et al*. (2014) Methane and carbon dioxide fluxes and their regional scalability for the European Arctic wetlands during the MAMM project in summer 2012. *Atmospheric Chemistry and Physics*, **14**, 13159-13174.

Phelps AR, Peterson KM, Jeffries MO (1998) Methane efflux from high-latitude lakes during spring ice melt. *Journal of Geophysical Research*, **103**, 29,029-29,036.

Rasilo T, Prairie YT, Del Giorgio PA (2015) Large-scale patterns in summer diffusive CH_4 fluxes across boreal lakes, and contribution to diffusive C emissions. *Global Change Biology*, **21**, 1124-1139.

Sabrekov AS, Runkle BRK, Glagolev MV, Terentieva IE, Stepanenko VM, Kotsyurbenko OR, Maksyutov SS, Pokrovsky OS (2017) Variability in methane emissions from West Siberia's shallow boreal lakes on a regional scale and its environmental controls. *Biogeosciences*, **14**, 3715-3742.

Sachs T, Wille C, Boike J, Kutzbach L (2008) Environmental controls on ecosystem-scale CH_4 emission from polygonal tundra in the Lena River Delta, Siberia. *Journal of Geophysical Research*, **113**, G00A03.

Sanden JJ van der, Drouin H, Hicks FE, Beltaos S (2009, June) Potential of RADARSAT-2 for Monitoring of River Freeze-up Processes. Paper presented at CGU HS Committee on River Ice Processes and the Environment, 15th Workshop on River Ice, St. John's, Newfoundland and Labrador.

Saunois M, Bousquet P, Poulter B *et al*. (2016). The global methane budget 2000-2012. *Earth System Science Data*, **8**, 697-751.

Schuur EAG, McGuire AD, Schädel C *et al*. (2015) Climate change and the permafrost carbon feedback. *Nature*, **520**, 171-179.

Smith LC, Sheng Y, MacDonald GM (2007) A First Pan-Arctic Assessment of the Influence of Glaciation, Permafrost, Topography and Peatlands on Northern Hemisphere Lake Distribution. *Permafrost and Periglacial Processes*, **18**, 201-208.

Taylor AE, Dallimore SR, Judge AS (1996) Late Quaternary history of the Mackenzie-Beaufort region, Arctic Canada, from modelling of permafrost temperatures. 2. The Mackenzie Delta – Tuktoyaktuk Coastlands. *Canadian Journal of Earth Sciences*, **33**, 62-71.

Thornton BF, Wik M, Crill PM (2016) Double-counting challenges the accuracy of high-latitude methane inventories. *Geophysical Research Letters*, **43**, 12,569-12,577.

Tuzson B, Hiller RV, Zeyer K, Eugster W, Neftel A, Ammann C, Emmenegger L (2010) Field intercomparison of two optical analyzers for CH_4 eddy covariance flux measurements. *Atmospheric Measurement Techniques*, **3**, 1519-1531.

Verpoorter C, Kutser T, Seekell DA, Tranvik LJ (2014) A global inventory of lakes based on high-resolution satellite imagery. *Geophysical Research Letters*, **41**, 6396-6402.

Walter Anthony K, Daanen R, Anthony P, Schneider von Deimling T, Ping C-L, Chanton JP, Grosse G (2016) Methane emissions proportional to permafrost carbon thawed in Arctic lakes since 1950s. *Nature Geoscience*, **9**, 679-682.

Walter Anthony KM, Anthony P, Grosse G, Chanton, J (2012) Geologic methane seeps along boundaries of Arctic permafrost thaw and melting glaciers. *Nature Geoscience*, **5**, 419-426.

Walter KM, Zimov SA, Chanton JP, Verbyla D, Chapin III FS (2006) Methane bubbling from Siberian thaw lakes as a positive feedback to climate warming. *Nature*, **443**, 71-75.

Wik M, Thornton BF, Bastviken D, Uhlbäck J, Crill PM (2016a) Biased sampling of methane release from northern lakes: A problem for extrapolation. *Geophysical Research Letters*, **43**, 1256-1262.

Wik M, Varner RK, Walter Anthony K, MacIntyre S, Bastviken D (2016b) Climate-sensitive northern lakes and ponds are critical components of methane release. *Nature Geoscience*, **9**, 99-106.

Wille C, Kutzbach L, Sachs T, Wagner D, Pfeiffer E-M (2008) Methane emission from Siberian arctic polygonal tundra: eddy covariance measurements and modeling. *Global Change Biology*, **14**, 1395-1408.

Yvon-Durocher G, Allan AP, Bastviken D *et al*. (2014) Methane fluxes show consistent temperature dependence across microbial to ecosystem scales. *Nature*, **507**, 288-295.